Received: 22 August 2021 | Revised: 4 January 2022 | Accepted: 8 January 2022

DOI: 10.1002/eqe.3602

RESEARCH ARTICLE

WILEY

Performance evaluation of seismically isolated buildings near active faults

Shoma Kitayama[1] | **Michael C. Constantinou**[2]

[1] School of Civil Engineering, University of Leeds, Leeds LS2 9JT, UK

[2] Department of Civil, Structural and Environmental Engineering, University at Buffalo, State University of New York, Buffalo, New York 14260, USA

Correspondence
Shoma Kitayama, School of Civil Engineering, University of Leeds, Leeds, LS2 9JT, UK.
Email: s.kitayama@leeds.ac.uk

Funding information
University at Buffalo

Abstract

This paper investigates the collapse risk of seismically isolated buildings that are designed by the procedures of the ASCE/SEI 7-16 standard for sites within 5 km of the active fault that controls the hazard. The study is based on six-story perimeter frame buildings designed with special concentrically braced frames for a location in California. The seismic isolation systems considered in this study are comprised of either: (i) triple friction pendulum bearings with high friction coefficients at the sliding interfaces, (ii) triple friction pendulum bearings with low friction coefficient at the sliding surfaces and enhanced with fluid viscous dampers, or (iii) triple friction pendulum bearings with low friction coefficients at the sliding surfaces. The paper demonstrates that the seismically isolated buildings designed per Section 17.3.3 in ASCE/SEI 7-16 standard, but with either increased isolator displacement capacity or increased superstructure strength by comparison to the minimum required, can achieve an acceptable collapse risk. It is also demonstrated that the seismic isolation systems that have the best collapse performance for far-field motions are not necessarily the best for the near-field pulse-like ground motions.

KEYWORDS

ASCE/SEI 7, near-field motions, performance evaluation, seismic isolation, triple friction pendulum, viscous dampers

1 | INTRODUCTION

The presence of velocity pulses in the ground motions (illustrated in Figure 1A) that are often produced when the fault ruptures towards a site (called "forward directivity effect"),[1] have been known to impose larger demands on structures than ground motions without velocity pulses[2–7, among many studies]. Thus, such pulse-like ground motions should be explicitly considered for the design of structures at near-fault regions as the pulse-like ground motions are generally anticipated in near-fault regions. As illustrated in Figure 1B, the pulse-like ground motions cause large demand on structures because the spectral acceleration of pulse-like ground motions becomes large at periods longer than 0.6 s and especially around the particular period that defines the pulse period, T_p[1,8]. Pulse-like ground motions are particularly important for the design of structures with a long effective period.

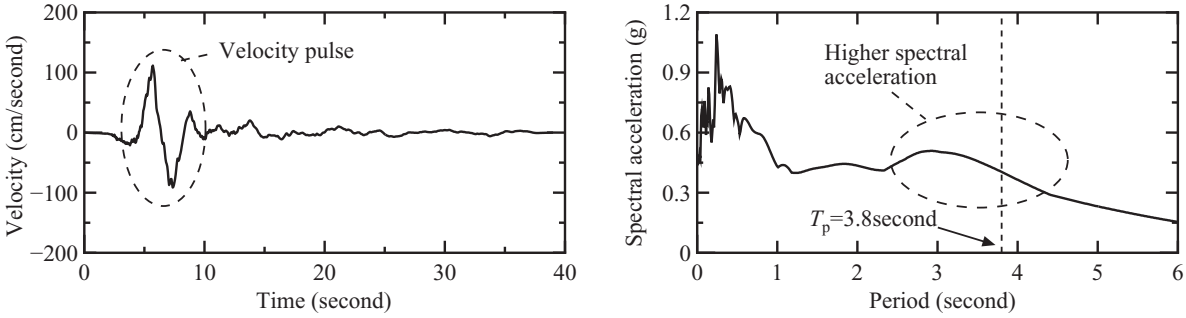

(A) Velocity time history of ground motion record (B) Pseudo acceleration spectrum

FIGURE 1 Example of pulse-like ground motion: (A) Velocity time history from 1979 Imperial Valley earthquake (El Centro Array #6), (B) 5%-damped acceleration spectrum of the same record

The current ASCE/SEI 7 standard (Section 17.3.3 in ASCE/SEI 7-16[9]) specifies that seismically isolated buildings located at near-field sites should be designed by considering larger seismic demands than the demand on structures at far-field sites by using a larger spectral acceleration. This modification of the design spectral acceleration is necessary as the current seismic hazard maps that are used to derive the design spectral acceleration in the seismic design standard[9] do not explicitly consider the collapse risk in the near-field region.[10]

A few studies investigated the seismic performance of seismically isolated buildings that were designed for near-field sites. Hall and Ryan[11] investigated the seismic performance of seismically isolated buildings designed per the 1997 Uniform Building Code (UBC). The study demonstrated that six-story seismically isolated buildings with moment-resisting frames might experience large inter-story drift under near-field pulse-like motions and drift is reduced when supplemental dampers are added alongside the isolators. Since this early study, the design standard updated the minimum requirements for the design of seismically isolated buildings at near-field sites, which is different from the ones in the 1997 UBC[12]. The design of seismically isolated buildings at near-field sites based on the current version of the ASCE/SEI 7-16 standard[9] is discussed in Section 3 in this paper, which then investigates the collapse risk of seismically isolated buildings that were designed for near-field sites based on ASCE/SEI 7-16 standard[9].

Previous studies by the authors[13,14] and others[15,16] investigated the collapse performance of seismically isolated buildings designed by the ASCE/SEI 7 standards[9,17] when located at far-field sites using the FEMA P695 procedures. Another study[19] focused on the collapse performance of sliding isolation bearings in buildings when subjected to recorded pulse-like motions but did not address the performance of the buildings designed based on the ASCE standard. A recent study by authors[20] observed that the probabilities of collapse in the lifetime of seismically isolated electrical transformers under the near-field ground motions did not substantially differ from the results of the same transformers under the far-field ground motions. This result appears in contradiction with the results of a study[21] that observed that the pulse-like ground motions induced larger isolator displacement demands than the non-pulse-like ground motions. However, the results are dependent on the definition of collapse and the displacement capacity of the isolators, which for the electrical transformer study[20] involved small displacement capacity isolators of interest to the US electric power industry, whereas in many studies for example[21], the isolators had unlimited displacement capacity. In the case of the electrical transformer study, "collapse" was controlled by equipment acceleration limits which were affected by impact on the restrainers of the small displacement capacity isolators.

Other studies[22,23] investigated the seismic response of seismically isolated structures under signal input (known as Ricker pulse[24]) that resembles pulse-like ground motions and observed a dependence of the response on the pulse period of pulse-like motions. Those observations are consistent with the studies of non-isolated buildings under pulse-like motions which have concluded that the largest structural seismic response occurs when the structural predominant period is near the pulse period[ex.,8,25–27]. One study[22] used simplified models for the isolators that did not account for their ultimate behaviour-particularly hardening and displacement restrainer effects, which are known to have an important effect on the collapse performance of seismically isolated buildings. Another study[23] focused on the mechanical behaviour of the seismic isolation bearings and did not examine the relationship between the collapse performance of seismically isolated buildings and pulse characteristics of ground motions. A recent study[30] also computed collapse probabilities of seismically isolated buildings for near-field ground motions but it differs from the study of this paper as (a) the design of the isolated buildings was based on the Equivalent Lateral Force (ELF) procedures of ASCE/SEI 7-16, whereas the study of this paper on response history analysis procedures (analysis and design was

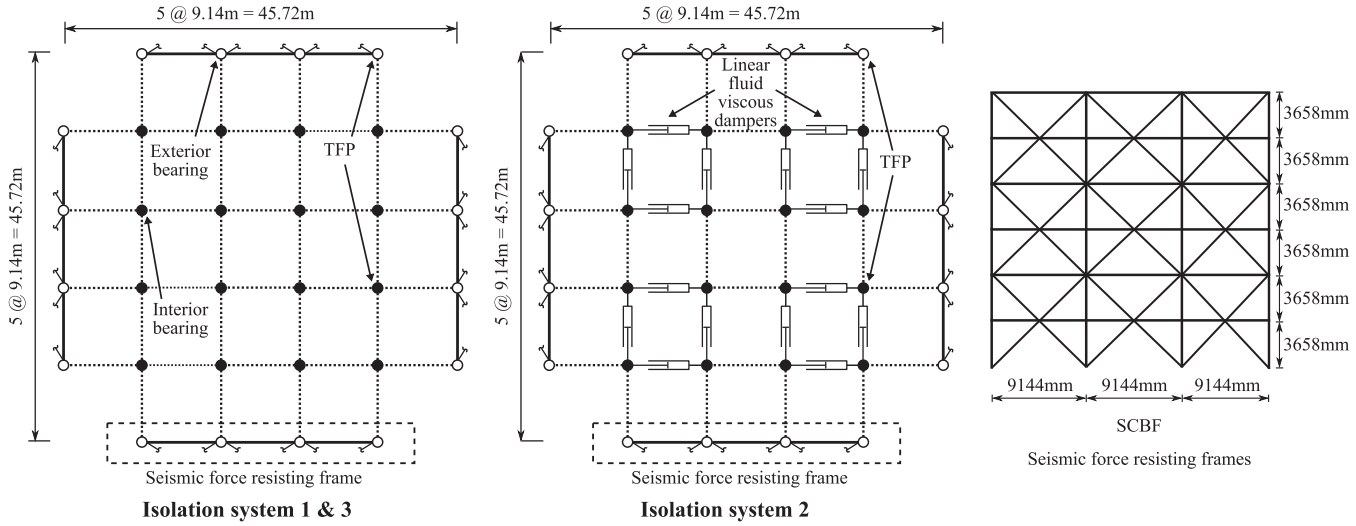

FIGURE 2 Building plan and elevations

based on the ELF procedure which is permitted for the structures considered, but response history analysis typically predicts larger displacements and forces for near-field conditions and thus prevails and should have been used), (b) the collapse performance evaluation followed the FEMA P-695 procedures,[18] whereas the study of this paper follows a different procedure that is suitable for near-field motions, and (c) the study did not use a probabilistic procedure to account for the occurrence of different pulse periods and the occurrence of pulse-like and non-pulse-like motions for seismic collapse assessment and only considered pulse-like ground motion records, which tends to result in overestimation of the collapse probabilities. Note that the FEMA P-695 procedure[18] for collapse performance assessment of buildings at near-field sites does not account for the distance to the fault, the occurrence of different pulse periods and the occurrence of pulse-like and non-pulse-like motions. The procedure used in this study accounts for these effects.

It is evident that further investigation is needed to understand the collapse performance of seismically isolated structures designed per specific standards in near-field sites and subjected to near field ground motions. This paper investigates the seismic performance of seismically isolated buildings designed by the procedures of Section 17.3.3 in ASCE 7-16[9] for seismically isolated buildings that are constructed at sites within 5 km of an active fault that controls the hazard. The performance assessment follows the approach proposed by Champion and Liel[27] to compute the probability of collapse of buildings. This approach incorporates the effects of pulse-like ground motions by considering the probability distributions of pulse-period and occurrence of pulse-like ground motions, which were not considered in previous studies[20,30]. This paper utilizes the same archetypical six-story buildings with perimetric steel special concentrically braced frames (SCBF) that has been previously used[13,14,28,29,31,32] but re-designed to be located at near-field sites. Moreover, the buildings designed for this study have superstructure strengths and isolation system capacities larger than the minimum requirements of ASCE/SEI 7-16. The seismic performance of seismically isolated buildings designed to just satisfy the minimum requirements of ASCE/SEI 7-16[9] was previously studied by authors[13,14,28,29] for far-field ground motions. Those studies showed that minimally designed seismically isolated buildings in the far-field might have unacceptable probabilities of collapse. Based on that experience, the buildings of this study were designed with enhanced requirements in order to achieve acceptable probabilities of collapse in the near-field.

2 | BUILDING DESIGNS AND SIMULATION MODELS

The building plan and elevations are shown in Figure 2. The total seismic weight of the buildings is 53,670 kN. The buildings are located on soil class D with MCE_R spectral acceleration values[9] of $S_{MS} = 1.5$ g and $S_{M1} = 0.9$ g and assumed to be located within 5 km of the active fault that controls the hazard. In earlier studies of the authors seismically isolated buildings were designed and analysed for a location having the same parameters but located in the far-field (specifically, located in San Francisco, CA, Latitude: 37.783°, Longitude: 122.392°). Risk Category is II per ASCE/SEI 7-16[9]. The isolation system consists of Triple Friction Pendulum (TFP)[33] isolators placed below each column and in one case viscous dampers

are used to enhance the isolation system. The analysis procedures for the design of seismically isolated buildings located at near-field sites is described in Section 17.3.3 in ASCE/SEI 7-16[9]. The procedures require the use of response history analysis with specially selected and scaled ground motions for the structures considered in this study. Analysis of the building was performed in program SAP2000[34] using seven pairs of ground motion records that were:

1. Rotated to the fault-normal (FN) and fault-parallel (FP) directions of the causative fault.
2. Scaled so that the average spectrum of the fault-normal components was not less than the MCE_R spectrum for the range between $0.2T_M$ (T_M: based on upper bound isolation system properties[9]) and $1.25T_M$ (T_M: based on lower bound isolation system property[9]).
3. Scaled so that the average spectrum of the fault-parallel components is not less than 50% of the MCE_R response spectrum for the range between $0.2T_M$ and $1.25T_M$.
4. Scaled such that in the period range between $0.75T_M$ and $1.25T_M$, the average of the SRSS spectra of the seven pairs does not fall below the corresponding ordinate of the response spectrum used in the design (MCE_R).

Three different seismic isolation systems were designed to meet and exceed the minimum requirements in Section 17.3.3 in ASCE/SEI 7-16[9] by modifying one of the seismic isolation systems that was originally designed for far-field conditions (TFP-3 in Refs. 13,14,28,29):

1. Isolation system 1: The isolators are triple friction pendulum bearings with the geometric properties of isolator TFP-3[13,14,28,29] but with increased friction values. The ultimate displacement capacity of this isolation system as finally configured is 973 mm.
2. Isolation system 2: The isolators are triple friction pendulum bearings with the geometric and frictional properties of isolator TFP-3[13,14,28,29] and with linear fluid viscous dampers added in the isolation system. The ultimate displacement capacity of this isolation system as finally configured is 973 mm.
3. Isolation system 3: The isolators are triple friction pendulum bearings with the geometric and frictional properties of isolator TFP-3[13,14,28,29] but with increased displacement capacity (all geometric properties are the same but the main concave plates are larger). The ultimate displacement capacity of this isolation system as finally configured is 1461 mm.

No moat walls were utilized in restraining the isolation system displacement. Also, the superstructure for each of the three isolation systems differed depending on the computed response and the selection of the R_I-factor[9] within the permitted range of 1–2. This will be discussed next.

Seven near-field ground motion records from the suite presented in FEMA P-695[18] were used. Information on the selected near-field ground motion records is presented in Table 1. The pulse-periods, T_p, for each direction and the classification (pulse or non-pulse) were obtained using a MATLAB code developed by Baker[35]. The table also presents the scale factors applied to each of the seven records for each of the three isolation systems. The scale factors differ as the effective periods[9], T_M, of the isolation systems differ. The scaled acceleration response spectra for each of the isolation systems are shown in Figure 3 to demonstrate that the scaling complies with the criteria of Section 17.3.3 in ASCE/SEI 7-16[9] as listed above. Note that these motions are only used in the analysis and design of the isolated buildings per ASCE/SEI 7-16. They are not used for the collapse performance evaluation that follows.

Figures 4 and 5 and Table 2 present drawings, force-displacement loops and lower and upper properties of the isolators and dampers for the three isolation systems. Isolation system 2 utilizes eight linear viscous dampers in each principal direction as shown in Figure 2. The dampers have a combined (total of eight devices) damping constant $C = 5.5$ kN s/mm in the lower bound condition and $C = 6.7$ kN s/mm in the upper bound condition. The range of properties corresponds to ±11% of the total nominal damping constant in each direction, which is consistent with the typical ±15% permitted variability for individual dampers. Quantity D_M is the average peak resultant isolator displacement computed in nonlinear response history analysis using the seven scaled ground motion records in Table 1. The geometry of each damper is based on the dampers that were used in the construction of the Washington Hospital Healthcare System (WHHS) in California, USA. Also note that the displacement capacity (D_{Cap} in Figure 5) of the dampers was selected to be just over 1.5 times the average peak isolator displacement D_M for the MCE_R earthquake[9] (800 mm capacity vs. 519 mm computed average displacement, D_M). Also, the ultimate force capacity ("Ultimate$F_{Tension}$" and "Ultimate$F_{Compression}$" in Figure 5) of dampers was assumed to be 2.25 times the computed average peak damper force in the MCE_R level earthquake. This is typical in the design of high-performance dampers. The ultimate behaviour of the fluid viscous dampers was modelled based on a previous study by authors.

TABLE 1 Characteristics of selected near-field ground motion records and scale factors for response history analysis

PEER record seq. no.[a]	Magnitude	Year	Earthquake name	Recording station	Source (Fault type)	Scale factors			T_p (second) FN	T_p (second) FP
						Case 1	Case 2	Case 3		
802	6.9	1989	Loma Prieta	Saratoga - Aloha	Strike-slip	2.50	2.50	2.60	4.47	NA[b]
165	6.5	1979	Imperial Valley-06	Chihuahua	Strike-slip	4.55	4.55	8.30	NA[b]	NA[b]
723	6.5	1987	Superstition Hills-02	Parachute Test Site	Strike-slip	1.00	1.30	1.90	2.28	NA[b]
821	6.7	1992	Erzican, Turkey	Erzincan	Strike-slip	1.30	1.55	2.20	2.65	2.16
160	6.5	1979	Imperial Valley-06	Bonds Corner	Strike-slip	3.30	3.80	4.03	NA[b]	NA[b]
1165	7.5	1999	Kocaeli, Turkey	Izmit	Strike-slip	3.45	3.60	3.90	NA[b]	NA[b]
1605	7.1	1999	Duzce, Turkey	Duzce	Strike-slip	1.60	1.59	1.10	NA[b]	5.57

[a]Record numbers of 160 and 165 are from "No Pulse Records" in FEMA P695[18]. Others are from "Pulse Records" in FEMA P695.[18] All motions are from "Near field record" in FEMA P695[18].

[b]"NA" means that the record was identified as non-pulse-like record per Baker.[35]

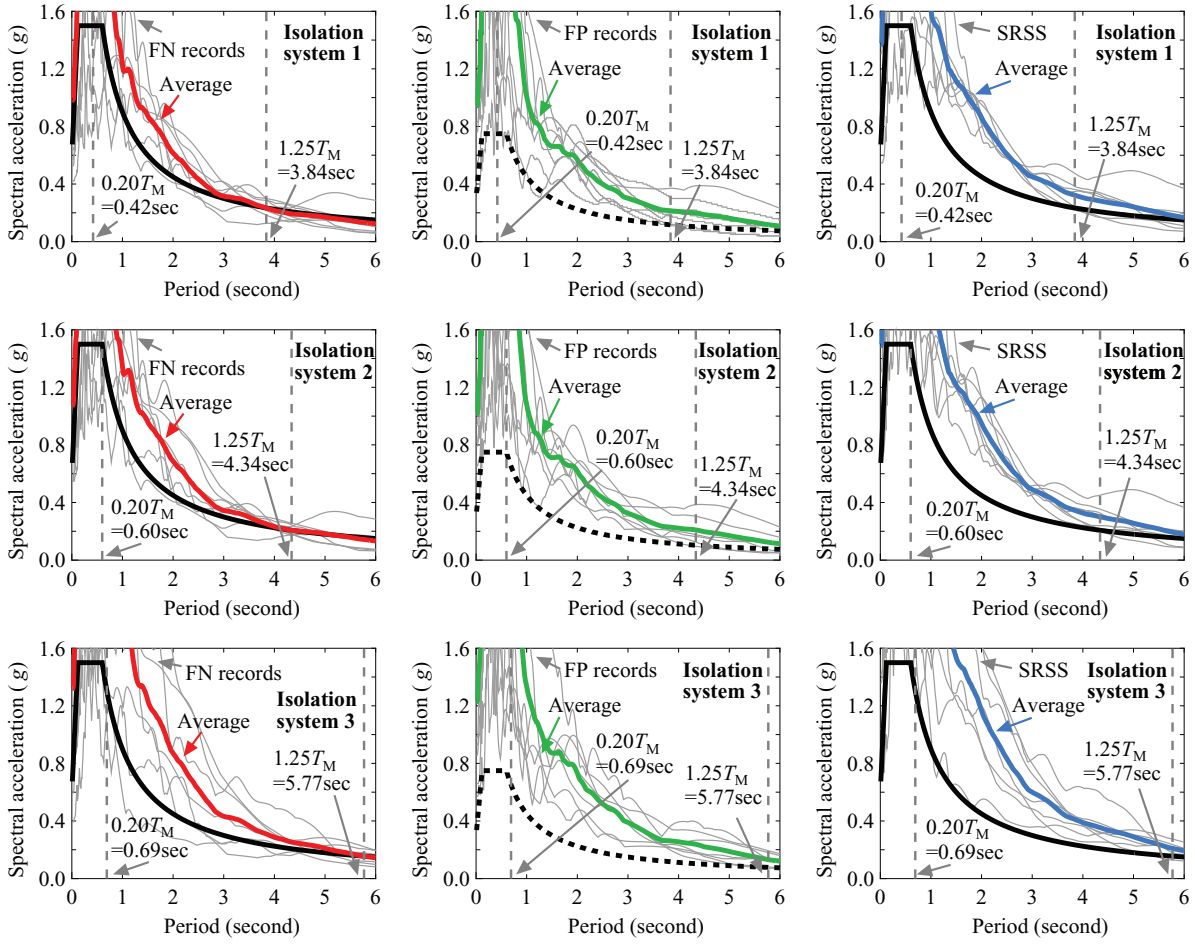

FIGURE 3 Acceleration response spectra of scaled near-field ground motion records

TABLE 2 Properties of seismic isolation systems

	$R_1 = R_4$ (mm)	$R_2 = R_3$ (mm)	$h_1 = h_4$ (mm)	$h_2 = h_3$ (mm)	D (mm)	$\mu_1 = \mu_4$	$\mu_2 = \mu_3$	F_I/W	F_{II}/W	$D_{Capacity}$ (mm)	$D_{Ultimate}$ (mm)
Isolation system 1	2235	305	114	76	419	0.080 (Lower bound, Interior) 0.100 (Lower bound, Exterior) 0.165 (Upper bound, Interior) 0.240 (Upper bound, Exterior)	0.020 (Lower bound, Interior & Exterior) 0.030 (Upper bound, Interior & Exterior)	0.273 (Lower bound) 0.374 (Upper bound)	0.596 (Lower bound) 0.606 (Upper bound)	825 (Lower bound) 867 (Upper bound)	973
Isolation system 2	2235	305	114	76	419	0.042 (Lower bound, Interior) 0.042 (Lower bound, Exterior) 0.087 (Upper bound, Interior) 0.101 (Upper bound, Exterior)	0.015 (Lower bound, Interior & Exterior) 0.022 (Upper bound, Interior & Exterior)	0.230 (Lower bound) 0.279 (Upper bound)	0.591 (Lower bound) 0.598 (Upper bound)	808 (Lower bound) 827 (Upper bound)	973
Isolation system 3	3962	305	114	76	660	0.042 (Lower bound, Interior) 0.042 (Lower bound, Exterior) 0.087 (Upper bound, Interior) 0.101 (Upper bound, Exterior)	0.015 (Lower bound, Interior & Exterior) 0.022 (Upper bound, Interior & Exterior)	0.209 (Lower bound) 0.258 (Upper bound)	0.571 (Lower bound) 0.578 (Upper bound)	1295 (Lower bound) 1314 (Upper bound)	1460

For isolation system 2: Linear viscous dampers, total $C = 5.5$ kN s/mm in each direction (Lower bound). Linear viscous dampers, total $C = 6.7$ kN s/mm in each direction (Upper bound).

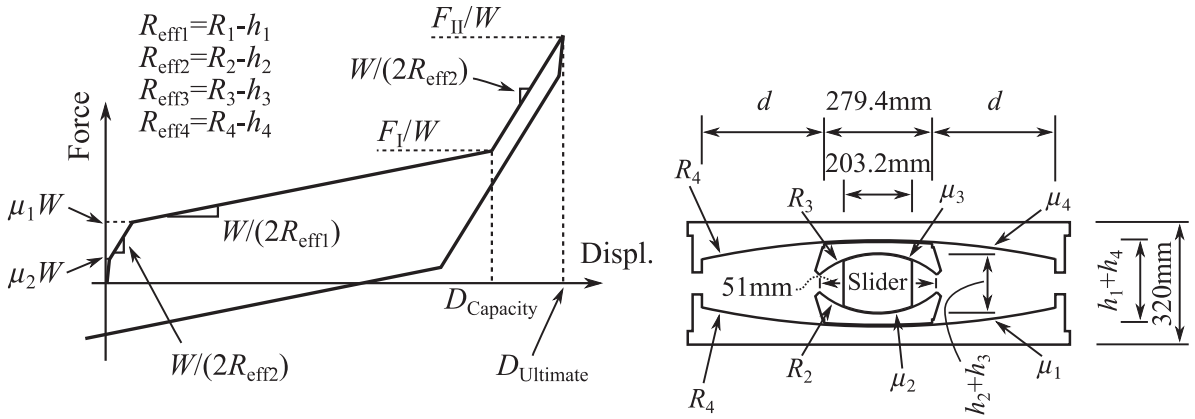

FIGURE 4 Geometry and properties of isolation bearings (Parameters are listed in Table 2)

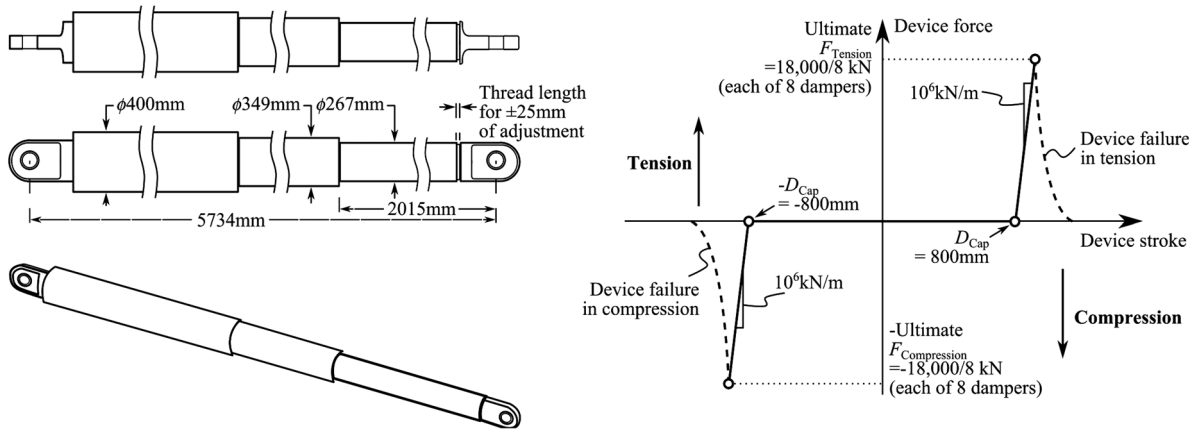

FIGURE 5 Geometry and ultimate properties of fluid viscous dampers in isolation system two

Note that the TFP isolators of isolation system 1 have a significantly higher friction coefficient than the other two isolation systems. Specifically, the important friction coefficient of surfaces 1 and 4 is 0.080 (interior isolators) and 0.100 (exterior isolators) in lower bound condition for system 1, whereas is 0.042 (interior & exterior isolators) for systems 2 and 3. The latter cases are common and supported by test data as presented in McVitty and Constantinou[32]. The higher friction values of system 1 (about twice as much as those of isolation systems 2 and 3 for the same pressure conditions) are possible[37] but are not based on actual testing of the specific bearings shown in Figure 4 and Table 2.

Table 3 presents the computed response and the selected design parameters of the three isolation systems and their corresponding superstructures. The isolator displacement capacities were selected so that $D_{Capacity}$ as shown in Figure 4 was larger than the maximum displacement D_M as computed by the procedures of ASCE/SEI 7-16 (average of seven response history analyses). This resulted in designs with enhanced displacement capacities by comparison to the minimum required by the ASCE standard[9].

Also, the response modification factor R_I for the design of the superstructure was selected in the range of 1.1–1.8 to represent designs ranging from "significantly enhanced superstructure strength" to "near-minimum superstructure strength". Also, the isolation system displacement capacity was selected in the range of $1.1D_M$–$1.6D_M$ to represent designs of "near-minimum isolator displacement capacity" to "significantly enhanced isolator displacement capacity". Note that the R_I factor was intentionally selected to have the values 1.1–1.8 so that the superstructure column, beam and brace sections are the same for all three isolation systems. Table 4 provides section information for braces/columns and beams of the seismic force-resisting system of the superstructure of the three isolation systems.

It is noted that the seismic performance of seismically isolated buildings designed to just satisfy the minimum requirements per ASCE/SEI 7-16[9] is out of the scope of the current study. The buildings designed for this study have superstructure strengths and isolation system capacities larger than the minimum requirements of ASCE/SEI 7-16[9]. The seismic performance of seismically isolated buildings designed to just satisfy the minimum requirements of ASCE/SEI 7-16[9] was

TABLE 3 Response and design parameters of isolation systems and corresponding superstructure

	Isolation system 1	Isolation system 2[a]	Isolation system 3
D_M	634 mm	519 mm	1159 mm
$D_{Capacity}$	825 mm = $1.3D_M$	808 mm = $1.6D_M$	1295 mm = $1.1D_M$
$D_{Ultimate}$	973 mm = $1.5D_M$	973 mm = $1.9D_M$	1460 mm = $1.3D_M$
T_M	2.101 s (Upper bound)	3.004 s (Upper bound)	3.465 (Upper bound)
	3.072 s (Lower bound)	3.473 s (Lower bound)	4.615 s (Lower bound)
Shear force demand for design	13,813 kN = $0.257W$	13,850 kN = $0.258W$	8830 kN = $0.165W$
R_I factor	$R_I = 1.8$	$R_I = 1.8$	$R_I = 1.1$
System description	Moderately enhanced isolator displacement capacity/near minimum superstructure strength	Significantly enhanced isolator displacement capacity/near minimum superstructure strength	Near minimum isolator displacement capacity/significantly enhanced superstructure strength

[a]For "Isolation system 2", dampers with combined $C = 5.5$ kN s/mm and $C = 6.7$ kN s/mm in each orthogonal direction are used for lower and upper bound analysis, respectively.

TABLE 4 Section of braces, columns and beams of superstructure

Story or floor		Section
Roof	Beams	W16 × 26
6	Columns	W12 × 35
	Braces	HSS4.5 × 0.337
	Beams	W16 × 26
5	Columns	W12 × 35
	Braces	HSS6 × 0.5
	Beams	W16 × 31
4	Columns	W12 × 58
	Braces	HSS7.5 × 0.5
	Beams	W16 × 31
3	Columns	W12 × 58
	Braces	HSS7.5 × 0.5
	Beams	W16 × 31
2	Columns	W12 × 96
	Braces	HSS8.625 × 0.5
	Beams	W16 × 31
1	Columns	W12 × 96
	Braces	HSS8.625 × 0.5
	Beams	W18 × 50

previously studied by authors[13,14,28,29] for far-field ground motions. Those studies showed that minimally designed seismically isolated buildings in the far-field may have unacceptable probabilities of collapse. Based on that experience, the buildings of this study were designed with enhanced requirements in order to achieve acceptable probabilities of collapse in the near-field.

The procedure for seismic collapse performance assessment is described next. Note that the procedure for the design of seismically isolated buildings for near-field sites (presented in this section) and the procedure for the collapse performance assessment of buildings are different. The former is described in Section 17.3.3 of ASCE/SEI 7-16[9] but the latter is not. The performance assessment procedure, presented in the next section, follows a methodology proposed by Champion and Liel[27]. Analyses for the collapse performance assessment were conducted with two-dimensional models of the buildings so that torsion could not be considered. Accordingly, the additional displacement capacity that isolators are provided with for accommodating torsion has been disregarded (that is, actual isolators and dampers should have been larger in capacity to accommodate torsion). As such, results are obtained on the required isolator displacement capacities as a function of

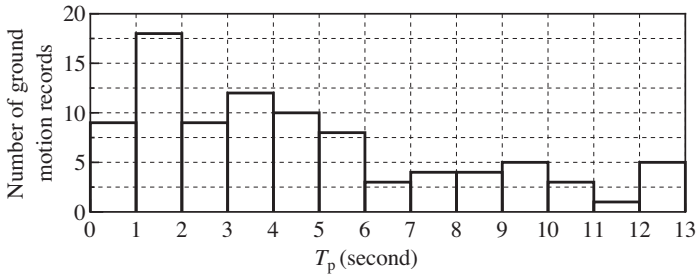

FIGURE 6 Distribution of pulse period T_p in pulse-like ground motion records (total number of records: 91)

D_M for achieving specific collapse risks. The analysis was performed in program OpenSees[38] including the gravity portion of the building. Details of the modelling are described in Kitayama and Constantinou.[13,14]

3 | GROUND MOTION RECORDS FOR COLLAPSE PERFROMANCE EVALUATION

3.1 | Near-field pulse-like ground motion record set

The 91 pulse-like ground motion records compiled by Baker[35] were used. All ground motions were recorded at sites located within 30 km from fault rupture, had a peak ground acceleration (PGA) larger than 0.1 g, a peak ground velocity (PGV) larger than 30 mm/s and a magnitude larger than 5.0. While more recent research by Shahi and Baker[39] identified a larger number of pulse-like ground motions from the recently updated Next Generation Attenuation-West 2 database[40], the number of ground motions[35] (=91) is deemed enough for this study based on the number of near-field ground motion records (56 records) used in FEMA P695[18] for seismic collapse evaluations of buildings. The pulse-like ground motions compiled in Baker[35] were classified based on the use of: (i) the size of the extracted velocity pulse (by wavelet analysis) relative to the original ground motion records, (ii) timing of pulse appearance in a record and (iii) absolute amplitude of the velocity pulse. The pulse period T_p was defined as the period associated with the maximum Fourier amplitude of the wavelet from ground motion records. Note that while some of the identified pulse-like ground motions[35] are likely not caused by directivity effects, those records are used in this paper by assuming that all pulse-like ground motions will cause similar effects regardless of their causal mechanism. Full detail of pulse-like ground motion records is available in Baker[35]. Figure 6 presents a histogram showing the relationship between the number of pulse-like ground motions (total 91) and period T_p.

3.2 | Far-field ground motion record set

This study also used a set of far-field ground motion records. The far-field ground motions were used to compute the collapse probability of buildings for near-field pulse-like ground motions. Note that this paper considers the probability of exceedance of observing pulse-like ground motions and non-pulse-like ground motions (i.e., far-field motions in this paper). Details are presented in Section 7 of this paper.

The suit of far-field motions used in the analysis is the set of 44 individual components of far-field ground motions utilized in the FEMA P695 project. The ground motions were all recorded at sites located at distance greater than or equal to 10 km from fault rupture, had a PGA larger than 0.2 g, a PGV larger than 150 mm/s and a magnitude larger than 6.5. Note that while Champion and Liel[27] observed that nine records out of the 44 far-field ground motions in FEMA[18] had pulses in the velocity time history that were removed from their study, this study uses all 44 far-field records as was done in other studies[41,42]. This was done in order to maintain a sufficient number of ground motion records in the far-field ground motion set. Also, as observed in Kitayama and Constantinou[20], the results of collapse performance evaluation of seismically isolated structures for near-field ground motions (half of the selected records had pulses) may not differ from the results of the same structures under far-field ground motions unless the pulse period T_p is properly accounted for in the performance assessment process. This observation supports the use of all 44 far-field records used in FEMA[18] for this study.

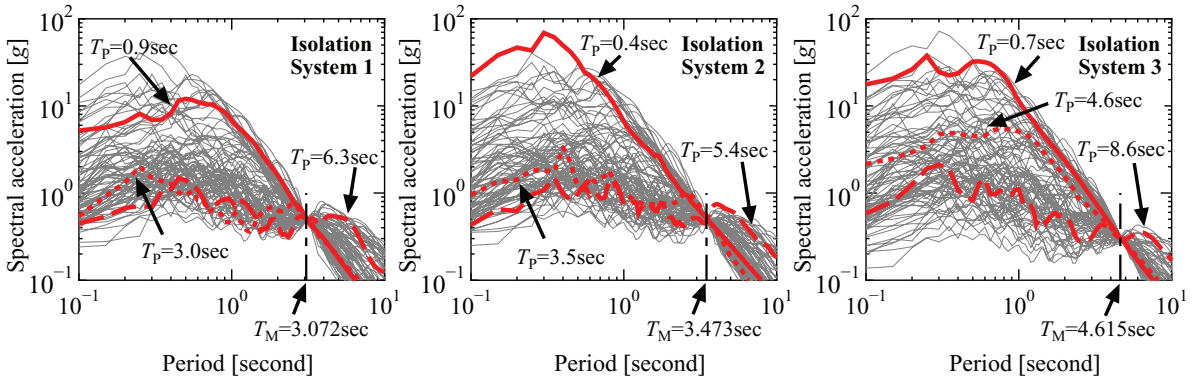

FIGURE 7 Acceleration response spectra (5%-damped) of pulse-like ground motion records for three isolation systems

4 | COLLAPSE ASSESSMENT APPROACH

The seismic collapse risk of the three isolated buildings was evaluated using incremental dynamic analysis (IDA)[43]. In the IDA, analysis is performed for the selected set of ground motion records with increasing intensity of each record. The intensity measure used in this paper is the spectral acceleration at the effective period of structures as reported in Table 2, $Sa(T_M)$. Also, the *Sa*-component approach was used for scaling the ground motion records (Appendix A13 in FEMA P-695[18]). This method is commonly used. In this method records are individually scaled according to $Sa(T_M)$ so that all records have exactly the same spectral acceleration at the period of interest. The nonlinear response analysis is terminated when the building collapses as described below. Hereafter the intensities of ground motions, $Sa(T_M)$ that cause a collapse of the buildings are denoted as $Sa_{Col}(T_M)$. The following collapse modes were considered in this study:

1. Collapse of the isolation system when the lateral displacement exceeds $D_{Ultimate}$ (see Figure 4 and Table 2).
2. The peak interstory drift of superstructure exceeded 0.05[45].
3. Instability as detected by termination of the analysis program.

Note that the TFP isolators lack an interior restrainer ring. This type of isolators is common nowadays and has been tested[46,47]. The bearing fails by exceeding the displacement limit when the rigid slider (the central part of TFP) slides off the inner concave plates. Uplift of the isolators was modelled but the uplift displacement was too small (much less than the height of the exterior ring of 38 mm) to cause disengagement of the bearing components as a result of the assumed high stiffness of the slab and girders above the isolators.

All results presented in this paper are for the lower bound conditions of the isolation systems (described in Figure 4 and in Table 2) as those resulted in the largest isolator displacement demands and the largest collapse probabilities. Figure 7 presents the spectral accelerations of the pulse-like records scaled to the intensities of $Sa(T_M) = 0.5$ g for isolation systems 1 and 2 and $Sa(T_M) = 0.35$ g for isolation system 3. These intensities are representative of the intensities that may cause a collapse of the buildings (see Section 5 in this paper). The figure also highlights three pulse-like records that have pulse-periods of $T_P < T_M$, $T_P \approx T_M$, and $T_P > T_M$. It is seen that the pulse-like records have large spectral acceleration at period T_P. It is also seen that because of the *Sa*-component scaling, the records with $T_P \approx T_M$ generally have smaller spectral acceleration than other records with $T_P \neq T_M$. The figure also shows that the spectra when $T_P >> T_M$ (long dashed lines) are close to the spectra when $T_p = T_M$ (short dotted lines). These observations are important in understanding the results of the collapse assessment that follows in the next section.

5 | INFLUENCE OF PULSE PERIOD ON PREDICTED COLLAPSE CAPACITY

Figure 8 presents the relationship between the collapse capacity of the three isolated buildings and period T_p divided by the effective period T_M for each pulse-like ground motion record. Note that the collapse capacity is the quantity $Sa_{Col}(T_M)$. Each data point (a total of 91 points in each graph) represents the collapse capacity for one of the pulse-like ground motion records obtained from the IDA[43]. A large value of $Sa_{Col}(T_M)$ indicates that the pulse-like ground motion record was scaled

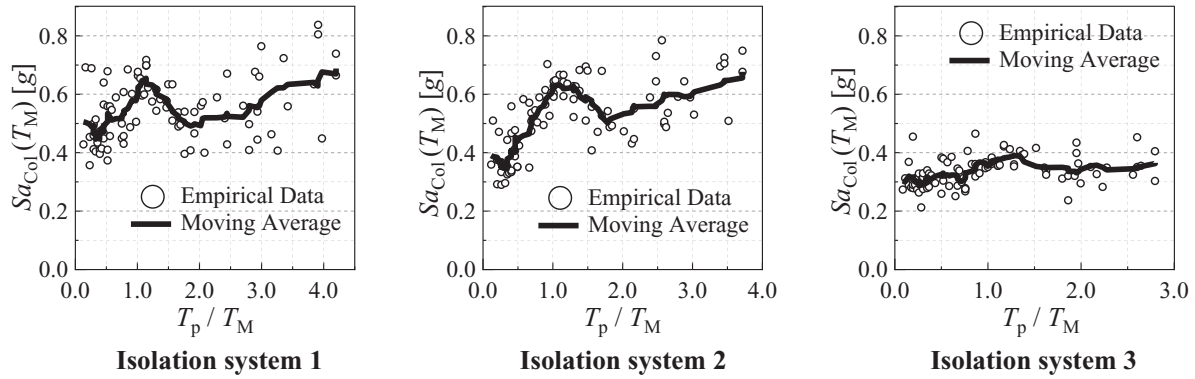

FIGURE 8 Collapse capacities of seismically isolated buildings as a function of T_p/T_M

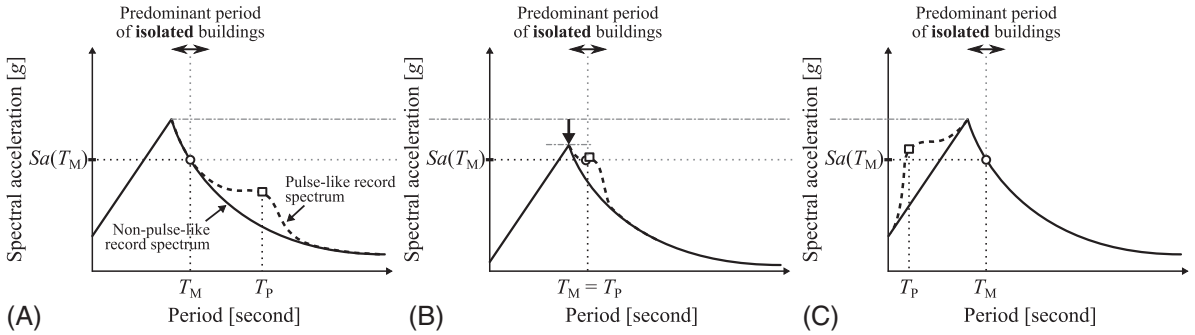

FIGURE 9 Relationship between T_M, T_P, and intensity of pulse-like records, $Sa(T_M)$: pulse-like record spectrum with: (A) T_P larger than T_M; (B) T_P equal to T_M; and (C) T_P smaller than T_M

to a higher intensity for collapse to occur. Figure 8 also shows the moving average of the empirical data, computed by averaging the point of interest with a window of length equal to 11 (=5 + 1 + 5) that includes the five points backwards, the point in the current position (=1), and the five points forward as done in Champion and Liel[27].

The shape of the moving average curve shows the impact of the value of T_P of pulse-like records, normalized by the effective period, on the collapse capacities of seismically isolated buildings. The moving average curves of isolated buildings have peaks at $T_p/T_M \approx 1$. This may be counter-intuitive as the acceleration response spectra of pulse-like records have peaks at T_p (see Figure 1B) and one may expect that the pulse-like records with $T_p/T_M \approx 1$ would cause larger seismic demand on the structures, leading to lower collapse capacities. The reason for the larger collapse capacities for $T_p/T_M \approx 1$ is due to the scaling method used in this study (*Sa*-component scaling – explained in the previous section). When this scaling method is used, each of the spectra is anchored at $T = T_M$, so that the peaks of the spectra are constrained at the value of $Sa(T = T_M)$. This makes the pulse-like records with $T_p/T_M \approx 1$ smaller than other pulse-like records with $T_p/T_M \neq 1$, as illustrated in Figure 9. Note that the peaks of moving average curves in Figure 8 occur at a period ratio slightly larger than $T_p/T_M = 1$. This is because the predominant period of the isolation systems considered under strong ground motions is larger than T_M and approaching a value based on the post-elastic stiffness (or sliding period) $T_{Slide} = 2\pi\sqrt{(2R_{effI}/g)}$, provided that the displacement is less than the stiffening displacement $D_{Capacity}$ per Figure 4—see Figure 10. We recognize that the scaling of the ground motions based on the spectral acceleration at period T_M instead of another, longer period (for example, the effective period at the displacement $D_{Capacity}$ per Figure 4 where stiffening occurs) may have an effect on the collapse performance-these effects are out of the scope of this study, although we do not expect such effects to be important given the small difference between displacements D_M and $D_{Capacity}$ (see Tables 2 and 3). For example, for system 1 $T_M = 3.07$ s ($D_M = 634$ mm) and the effective period at displacement $D_{Capacity} = 825$ mm is 3.49 s (for the critical lower bound conditions). For displacements larger than $D_{Capacity}$, the effective period is less than 3.49 s due to stiffening of the isolators (it is 2.56 s at the isolator's ultimate displacement of 973 mm).

When T_p/T_M becomes much larger than unity ($T_P/T_M >> 1$), the peaks of the moving average curves approach the peak at $T_P/T_M \approx 1$. This is because the effect of scaling of the records on structural collapse diminishes as T_P and T_M separate far away from each other. This may be also understood from another perspective as shown in Figure 7; the spectra with

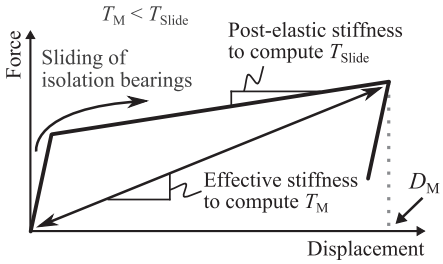

FIGURE 10 Predominant period of isolated structures

TABLE 5 Results of collapse capacity for different pulse periods for buildings

		Pulse-like records					
		$Sa_{Col}(T_M)$ [g]				Far-field records	
	T_M (s)	At $T_p = 0.5T_M$	At $T_p = 1.0T_M$	At $T_p = 3.0T_M$	β_{RTR}	$Sa_{Col}(T_M)$ [g]	β_{RTR}
Isolation system 1	3.072	0.502	0.594	0.580	1.061	0.690	0.249
Isolation system 2	3.473	0.443	0.614	0.602	1.179	0.669	0.260
Isolation system 3	4.615	0.322	0.354	N/A (See Figure 8)	0.981	0.387	0.184

$T_P \approx T_M$ (short dotted lines in Figure 7) and with $T_P >> T_M$ (long dashed lines in Figure 7) are close to each other. This is the result of the bulge of acceleration spectra at T_p occurring away of the period range that influences the collapse capacity of seismically isolated buildings.

Table 5 summarizes the collapse capacity results for the seismically isolated buildings, subjected to the pulse-like ground motion set. The collapse capacity is reported for multiple pulse periods (expressed as $T_p = kT_M$) to reflect the distinct regions of response in Figure 8. The median collapse capacity obtained from analysis of the far-field ground motion set is also provided for comparison. Note that the median collapse capacity obtained in analysis using the far-field ground motion database has been adjusted for spectral shape effects following Haselton et al.[48]—this adjustment was not needed for the results of the analysis using the near-field motions (the reason for this is discussed in the next section). Previous works by authors[13,14] and others[48] demonstrated that the probability of collapse would be overestimated without adjustments for the spectral shape effect. Details of the method of the adjustment of the median collapse capacities obtained in analysis using the far-field ground motions was described in Kitayama and Constantinou[13,14]. It is seen in Table 5 that the collapse capacities computed for pulse-like motions are generally smaller than the collapse capacities from far-field motions, especially at $T_p/T_M \neq 1$ for all buildings considered in this paper.

Table 5 also presents data on the record-to-record variability (dispersion coefficient β_{RTR}) computed in the analysis. For the case of near-field, pulse-like motions, β_{RTR} was computed by: (i) computing the difference between the collapse spectral acceleration for a given record and the moving average collapse capacity at that pulse period (this difference is called 'residual' collapse capacity), (ii) computing the natural logarithms of each of the absolute values of the residual collapse capacities, and (iii) taking the standard deviation of the natural logarithm of the residual collapse capacities. The computed values of the dispersion coefficient for near-field ground motions are much larger than the ones computed using the far-field ground motions, for which the computation is simpler and described in many studies[13,14,18]. The values of the dispersion coefficient computed using the near-field ground motions are provided for information only—they have not used in the computation of the probabilities of collapse. Also, they have not been used in the construction of collapse fragility curves, instead, the dispersion coefficient values computed for the far-field ground motions in Table 5 were used for the construction of the fragility curves as done in the past studies.[27,41,42]

6 | GROUND MOTION SCALING AND SPECTRAL SHAPE

This study used IDA[43] to compute the intensities of ground motions that cause collapse of three seismically isolated buildings. The ground motions were scaled up (often with large factors) and nonlinear response history analysis was conducted for increasing intensities until collapse of the buildings were detected. Since the ground motion characteristics (e.g., frequency content) differ depending on the intensity of motions[49], and IDA does not account for this, this section

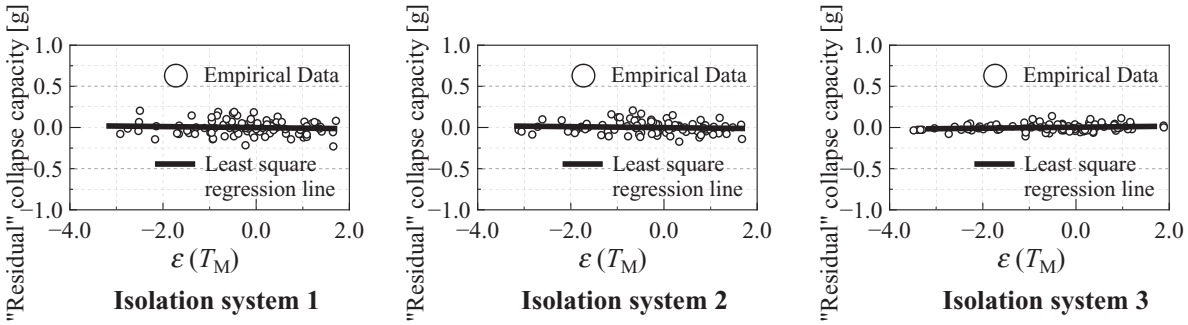

FIGURE 11 'Residual' collapse capacities of isolated buildings as a function of ground motion parameter $\varepsilon(T_M)$

examines the possibility that the pulse-like ground motions scaled with large factors might introduce bias in the collapse capacities. The procedure described in Baker[50], Baker and Cornell[51] and Champion and Liel[27] is used to examine the relationship between $\varepsilon(T_M)$ and the "residual" collapse capacity for the buildings. Quantity $\varepsilon(T_M)$ is an indirect measure of the spectral acceleration shape and is computed as the number of standard deviations between the observed spectral value (i.e., spectral acceleration of the original ground motion records) and the median value from a ground motion prediction equation. The residual collapse capacity was defined in the last paragraph in Section 5 of this paper. The residual collapse capacity assumes large values when the pulse period T_p and quantity $Sa(T_M)$ are insufficient measures to compute the collapse capacity. When there is a small dependency of the residual collapse capacity on changes in $\varepsilon(T_M)$, it is considered that the use of IDA does not introduce bias on the computed collapse capacities. In case the bias is found to be significant, the effect of $\varepsilon(T_M)$ on the collapse capacity may be accounted for using the procedures in Appendix A of FEMA[18]. The ground motion prediction equations developed by Boore and Atkinson[52] were used to compute $\varepsilon(T_M)$ in this study for consistency with the probabilistic seismic hazard analysis implemented in this study (discussed later in this paper).

Figure 11 presents the relationship between $\varepsilon(T_M)$ and the residual collapse capacity for the three seismically isolated buildings. The figure shows that there is no dependency of the residual collapse capacity and $\varepsilon(T_M)$. This suggests that a collapse assessment based on both T_p and $Sa(T_M)$ accounts for the spectral shape without introducing significant biases due to the ground motion scaling.

7 | SEISMIC COLLAPSE RISK AT NEAR-FIELD SITES

7.1 | Probability of collapse for near-field pulse-like ground motions

The collapse capacity of seismically isolated buildings at a near-field site depends on the ground motion intensity and the pulse period T_p. Based on Champion and Liel[27], the probability of collapse for a given spectral acceleration, $P[\text{Col}|Sa(T_M) > x]$, is given by:

$$\begin{aligned} P\ [\text{Col}|Sa\,(T_M) > x] = \ & P\,[\text{Col}|Sa\,(T_M) > x, \text{Pulse}] \cdot P\,[\text{Pulse}|Sa\,(T_M) > x] \\ & + P\,[\text{Col}|Sa\,(T_M) > x, \text{NoPulse}] \cdot P\,[\text{NoPulse}|Sa\,(T_M) > x] \end{aligned} \quad (1)$$

In this equation, $P[\text{Col}|Sa(T_M) > x, \text{Pulse}]$ is the probability of exceedance of collapse limits (presented in Section 4) given the intensity $Sa(T_M) > x$ when the pulse occurs; $P[\text{Pulse}|Sa(T_M) > x]$ is the probability of exceedance of observing pulse-like ground motion given the intensity $Sa(T_M) > x$; $P[\text{Col}|Sa(T_M) > x, \text{NoPulse}]$ is the probability of exceedance of collapse limits given the intensity $Sa(T_M) > x$ when a pulse does not occur; and $P[\text{NoPulse}|Sa(T_M) > x]$ is the probability of exceedance of not-observing pulse-like ground motion given the intensity $Sa(T_M) > x$. Note that $P[\text{NoPulse}|Sa(T_M) > x] = 1 - P[\text{Pulse}|Sa(T_M) > x]$.

In this study, $P[\text{Col}|Sa(T_M) > x, \text{NoPulse}]$ is computed from the collapse fragility analysis for the far-field records. It is computed using the median collapse capacity (adjusted for spectral shape based on Haselton et al.[48] and the dispersion factors reported in Table 5). The method of computation of quantity $P[\text{Col}|Sa(T_M) > x, \text{NoPulse}]$ was previously reported in Kitayama and Constantinou[13,14] and is also used in this study.

$P[\text{Col}|Sa(T_M) > x, \text{Pulse}]$ is computed by considering that the collapse capacities of the seismically isolated buildings are dependent on the pulse period and the relative likelihood of occurrence of each value of period T_p for different intensities[27]:

$$P\ [\text{Col}|Sa\,(T_M) > x, \text{Pulse}] = \sum_{i=1}^{\text{All } T_p} P\left[\text{Col}|T_p = t_i, Sa\,(T_M) > x, \text{Pulse}\right] \cdot P\left[T_p = t_i|Sa\,(T_M) > x, \text{Pulse}\right] \tag{2}$$

where $P[T_p = t_i|Sa(T_M) > x, \text{Pulse}]$ is the probability of observing $T_p = t_i$ of a pulse-like motion given the intensity of $Sa(T_M) > x$ when the pulse motion occurs and $P[\text{Col}|T_p = t_i, Sa(T_M) > x, \text{Pulse}]$ is the probability of collapse given a specific pulse period $T_p = t_i$ and intensity $Sa(T_M) > x$, when a pulse-like motion occurs. This probability is obtained from the moving average curves that were developed in the previous section of this paper for different cases of buildings (Figure 8). Also, $P[\text{Col}|T_p = t_i, Sa(T_M) > x, \text{Pulse}]$ is the log-normal cumulative distribution function with the median obtained from the moving average curve at $T_p = t_i$, $Sa_{Col}(T_M|T_p = t_i)$, and a total system uncertainty, computed as follows[18]:

$$\beta_{TOT} = \sqrt{\beta_{DR}^2 + \beta_{TD}^2 + \beta_{MDL}^2 + \beta_{RTR}^2} \tag{3}$$

where β_{DR} is the design requirements-related collapse uncertainty, β_{TD} is the test data-related collapse uncertainty and β_{MDL} is the modelling-related collapse uncertainty. For the seismically isolated structures with SCBF, the following quality ratings and related uncertainties were used: Good with $\beta_{MDL} = 0.2$ for modelling; good with $\beta_{TD} = 0.2$ for test data and superior with $\beta_{DR} = 0.1$ for design requirements (same assumptions made in FEMA[18] and Masroor and Mosqueda[16]). Quantity β_{RTR} is the record-to-record uncertainty that is computed as the standard deviation of the natural logarithm of absolute differences between moving average curves and the empirical data of the 91 records used in the analysis (listed in Table 5) based on Champion and Liel.[27] Note that in this study, the values of β_{RTR} obtained for far-field conditions were used following the previous studies by others[27,41,42]—this was the case for the results of this study. Finally, $P[\text{Col}|T_p = t_i, Sa(T_M) > x, \text{Pulse}]$ in Equation (2) is given by the following equation:

$$P\ \left[\text{Col}|\ T_p = t_i\ , Sa\,(T_M) > x, \text{Pulse}\right] = \int_0^x \frac{1}{s\beta_{TOT}\sqrt{2\pi}} \exp\left[-\frac{\left\{\ln s - \ln Sa_{Col}\left(T_M|T_p = t_i\right)\right\}^2}{2\beta_{TOT}^2}\right] \tag{4}$$

The probabilities $P[\text{Pulse}|Sa(T_M) > x]$ in Equation (1) and $P[T_p = t_i|Sa(T_M) > x, \text{Pulse}]$ in Equation (2) are obtained through de-aggregation in the probabilistic seismic hazard analysis (PSHA) that is described next.

7.2 | Probabilistic seismic hazard analysis that accounts for pulse-like ground motions

Generally, probabilistic seismic hazard analysis (PSHA) integrates over all possible earthquake ground motions at a site to develop a composite representation of the spectral amplitudes (i.e., intensity $Sa(T_M)$ in this study) and hazards (annual frequencies of exceedance)[53]. It has been proposed that the PSHA framework incorporates the effect of near-field pulse-like motions in seismic hazard assessment[54]. A recent study by Shahi and Baker[39] extended the work[54] and proposed equations for computing pulse-related parameters by using ground motion data from the NGA database[55]. The following equation computes the annual frequency of exceedance of particular intensity levels of ground motions that account for the occurrence of pulse-like ground motions[39]:

$$\lambda_{Sa(T_M)>x} = \sum_{i=1}^{N} \nu_i \iiint P^*\left[Sa\,(T_M)\,|m, r, z\,\right] \cdot f_i\,(m, r, z) \cdot dm \cdot dr \cdot dz \tag{5}$$

where ν_i is the mean rate of occurrence of earthquakes on a nearby fault i, N is the number of nearby faults, m is the magnitude, r is the distance, z represents the source-to-site geometry (see Figure 4 in Shahi and Baker[39]) and $f_i(m, r, z)$ is the probability density of occurrence of an earthquake with m, r and z on a particular fault i. Quantity $P^*[Sa(T_M)|m, r, z]$ is the probability of exceeding an intensity $Sa(T_M)$ given the occurrence of m, r and z, which is obtained by using the modified ground motion prediction equations considering pulse-like ground motions developed by Shahi and Baker.[39]

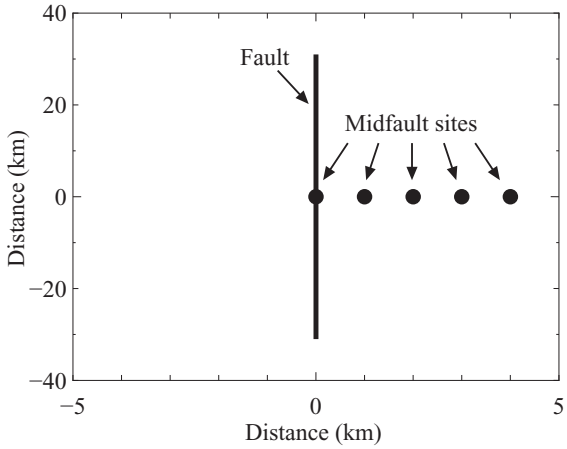

FIGURE 12 Assumed near-field site locations in relation to fault

Note that $P[\text{Pulse}|Sa(T_M) > x]$ in Equation (1) and $P[T_p = t_i|Sa(T_M) > x, \text{Pulse}]$ in Equation (2) are obtained from de-aggregation of the PSHA that accounts for pulse-like ground motions as follows[27,39]:

$$P\ [\text{Pulse}\,|Sa\,(T_M) > x\,] = \lambda_{Sa(T_M)>x,\text{Pulse}}/\lambda_{Sa(T_M)>x,\ \text{Total}} \tag{6}$$

$$P\left[\,T_p = t_i\ \,|Sa\,(T_M) > x\ ,\text{Pulse}\right] = \lambda_{Sa(T_M)>x,\text{Pulse},T_p=t_i}/\lambda_{Sa(T_M)>x,\text{Pulse}} \tag{7}$$

where $\lambda_{Sa(TM)>x,\text{Pulse}}$ is the rate of $Sa(T_M) > x$ when only pulse-like ground motions are considered, $\lambda_{Sa(TM)>x,\text{Total}}$ is the rate of $Sa(T_M) > x$ when all (i.e., both near-field pulse-like and non-pulse-like) ground motions are considered and $\lambda_{Sa(TM)>x,\text{Pulse},Tp=\ ti}$ is the rate of $Sa(T_M) > x$ when only pulse motions are considered and the pulse period becomes $T_p = t_i$.

7.3 | Implementation of PSHA

PSHA was conducted using site and fault parameters that were chosen to mimic the conditions at site that experienced pulse-like ground motions during the 1979 Imperial Valley earthquake based on Shahi and Baker[39]. To demonstrate the effects of the site-to-source geometry and variations in structural design on the seismic collapse performance of the seismically isolated buildings in the near-field region, we consider sites located near the assumed strike-slip fault as shown in Figure 12, with site-to-source distances ranging from 0 to 4 km at the midpoint close to a fault line. Previous studies[27,41,42] observed that the seismic response was not influenced by the position of the site relative to the fault axis. These studies also found that the parameter that was most influential on the collapse performance of buildings was the distance to the fault rupture. Thus, this study only considers "mid-fault" sites with different site-to-source distances (see Figure 12). The single fault length of 62 km with the recurrence rate of 0.09 earthquakes per year was assumed ($\upsilon_{i\ =1} = 0.09$ in Equation (5)) based on Champion and Liel[27]. Earthquakes of magnitude 5–7 were considered, and the magnitude recurrence relationship of the bounded Gutenberg-Richter model[56,57] was used to model the probability distribution of magnitudes. Such a recurrence model has also been recently used by Eads et al.[58]. The earthquake epicentre was assumed to be equally likely located at all locations along the fault[56]. Hazard analysis was performed for a strike-normal orientation at the site. The computed values of $\lambda_{Sa(TM)\ >\ x}$ in Equation (5) are presented in Figure 13 (top row). The de-aggregation of PSHA gives the $P[\text{Pulse}|Sa(T_M) > x]$ in Equation (1) and $P[T_p = t_i|Sa(T_M) > x, \text{Pulse}]$ in Equation (2) which are also presented in Figure 13 (middle and bottom rows). Note that this study only considered a single fault that mimics the site of the 1979 Imperial Valley earthquake. We assumed that the effect of near-field ground motions on the seismic performance of seismically isolated buildings is similar when different faults are used. In fact, the only differences when different faults are used are the probabilities of observing different pulse-periods (i.e., $P[T_p = t_i|Sa(T_M) > x, \text{Pulse}]$ in Equation (7)) and the probability of observing pulse-like ground motions (i.e., $P[\text{Pulse}|Sa(T_M) > x]$ in Equation (6)).

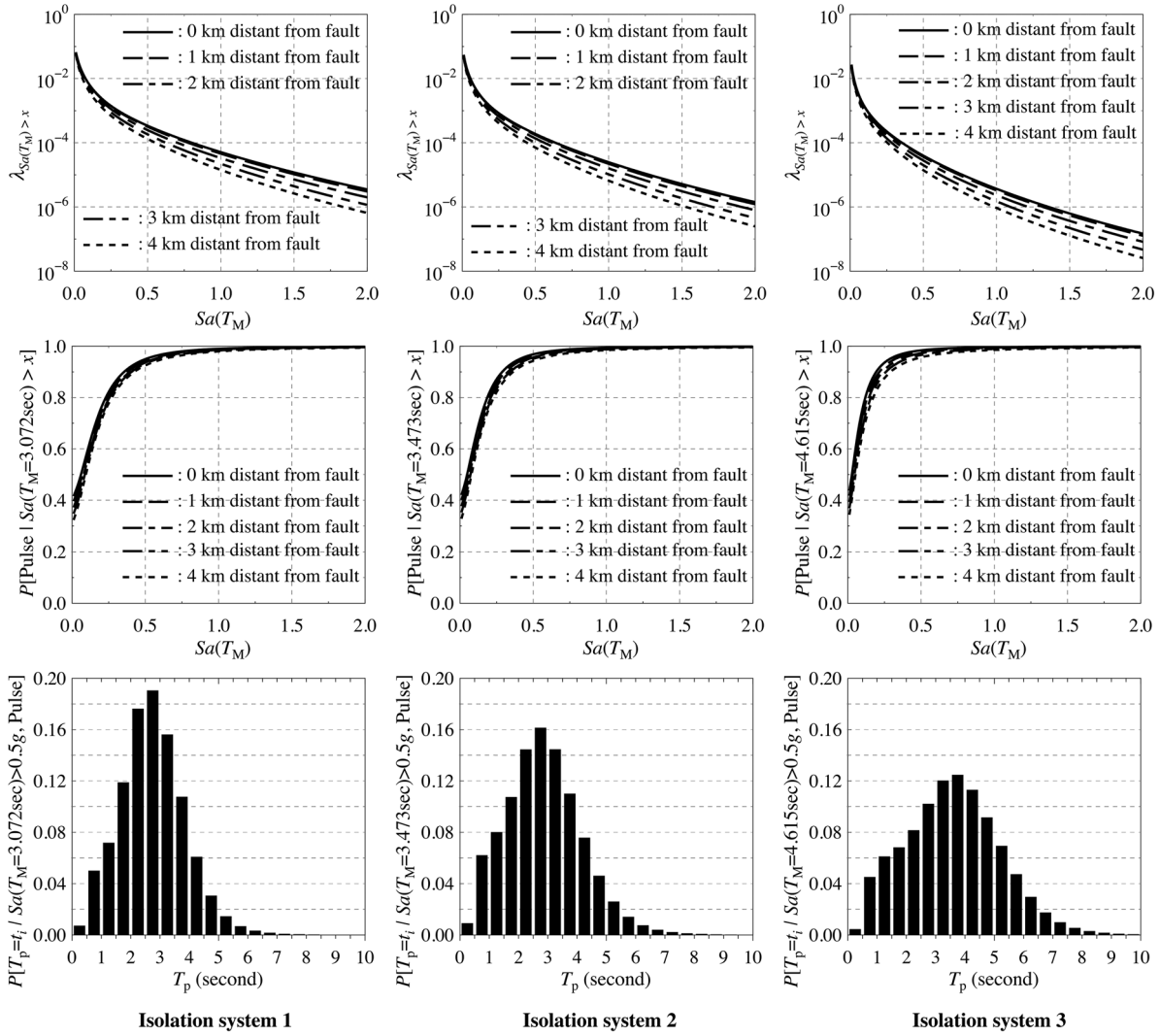

FIGURE 13 Results of PSHA: (Top row) seismic hazard curves with varying site-to-source distances; (Middle row) probability of pulse occurrence for the different mid-fault sites; (Bottom row) pulse period distribution for hazard levels that are representative of intensity measure causing a collapse of buildings at the 2 km fault site

7.4 | Collapse risk assessment

We described earlier in this paper the computation of the probability of collapse for different intensities to appropriately account for the near-field pulse-like ground motions based on the approach of Champion and Liel[27]. The collapse fragility curves per Equation (1) were computed and are presented in Figure 14 for different site-to-source distances. Figure 14 also includes the collapse fragility curves for far-field ground motions. Note that in the generation of the fragility curves for near-field ground motions, we used in Equation (3) the value of the dispersion coefficient β_{RTR} that was computed for the far-field motions as the β_{RTR} computed for near-field ground motions (reported in Table 5) was large and its use resulted in values of the probability of collapse much larger than those computed by the approach of Champion and Liel[27]. This observation and substitution was also made in other studies[27,41,42].

It is seen in Figure 14 that the collapse fragility curves for distances of 0–4 km have very small differences, while there are distinct differences between the fragility curves for near-field and far-field ground motions. However, the fragility curves of the three isolation systems are not directly comparable as the three systems have different effective period T_M.

The computed fragility curves based on Equation (1) were further utilized to obtain the probabilities of collapse given the occurrence of the maximum considered earthquake (MCE_R) to determine whether the probabilities of collapse are acceptable. These probabilities were computed by substituting parameter x in Equation (1) with the spectral acceleration of the risk-targeted maximum considered earthquake (MCE_R[9]) at the period of T_M, $Sa_{MCER}(T_M)$, for each seismic isolation

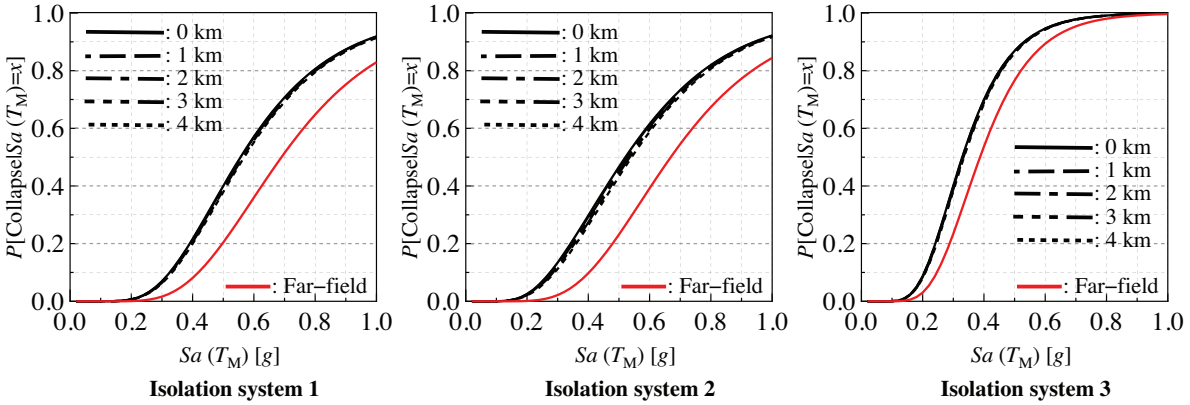

FIGURE 14 Collapse fragility functions for seismically isolated buildings at three different mid-fault sites. The far-field collapse fragility curve is provided for comparison

TABLE 6 Probabilities of collapse given the maximum earthquake

Structural systems	Probabilities of collapse in MCE_R (%)					
	At 0 km	At 1 km	At 2 km	At 3 km	At 4 km	Far-field
Isolation system 1	6.29	6.16	5.99	5.81	5.60	1.42
Isolation system 2	8.00	7.77	7.40	6.98	6.54	0.85
Isolation system 3	7.83	7.69	7.52	7.33	7.12	2.65

systems considered (i.e., $x = Sa_{MCER}(T_M = 3.072\text{ s}) = 0.293$ g for isolation system 1; $x = Sa_{MCER}(T_M = 3.473\text{ s}) = 0.259$ g for isolation system 2; $x = Sa_{MCER}(T_M = 4.615\text{ s}) = 0.195$ g for isolation system 3). The probabilities of collapse for MCE_R for the three isolated buildings are listed in Table 6. The results in Table 6 show acceptable probabilities of collapse (less than 10% given the MCE_R for risk category II buildings per Section 1.3.1.1 of ASCE/SEI 7-16[9]) for all isolation systems and all distances to the fault and with slightly increasing collapse risk as the site-to-source distance decreases. The effect of near-field ground motions in comparison with far-field motions on the collapse risk is evident in the significantly lower probabilities of collapse when the isolated structures, designed for near-field ground motions, were analysed for far-field motions. Past studies (other than the work of Hall and Ryan[11]) investigated the performance of seismically isolated buildings using near-field pulse-like ground motions but with the buildings (superstructure and isolation system) designed for far-field ground motions. This led to conclusions that isolated buildings do not perform as well for near-field as they do for far-field ground motions—a conclusion affected by the fact that the isolated buildings were not properly analysed and designed for the effects of near-field ground motions.

Interestingly, the computed probabilities of collapse for near-field motions are very close for the three isolation systems, despite significant differences in their design parameters. Yet there are some interesting observations. One would have expected isolation system 2 to outperform isolation system 1 due to the R_I factor being the same in the two designs but the isolator displacement capacity, by comparison to D_M, is larger in isolation system 2 than isolation system 1. The results in Table 6 show the opposite although the differences are small. However, the important observation is that isolation system 2 is more expensive (added dampers) for no benefit in the collapse performance. Apparently, the use of higher friction in isolation system 1 is equally or slightly more effective than adding linear viscous damping in isolation system 2 for restraining the isolator displacements. Also, one would have expected that isolation system 3 to have lower probabilities of collapse than the other systems due to the small value of the R_I factor used (1.1 vs. 1.8 in the other designs). However, the collapse was controlled by the failure of the isolators due to excessive displacement demand in the small displacement capacity isolators used (capacity equal to $1.1D_M$). It is also observed that the lowest probability of collapse for far-field motions was achieved by isolation system 2 while the lowest probability of collapse for near-field motions was achieved by isolation system 1 (at 0 km from fault). That is, the best isolator design for far-field sites is not necessarily the best for near-field sites in reducing the probability of collapse of seismically isolated buildings.

Note that the results for the case of the "Far-field" in Figure 14 and in Table 6 are the results of collapse performance assessment of the seismically isolated buildings designed for the near-field site but assessed using far-field ground motion records.

While this study focused on the collapse performance of seismically isolated buildings, other demand parameters such as floor accelerations, interstory drift ratios and residual story drift ratios are also important indicators of performance of buildings[29,59]. The findings and recommendations in this paper are only relevant when considering seismic collapse, whereas consideration of other performance indicators, of lifetime behavior[32,37] of the isolation system, other hazards and cost[60] may lead to different conclusions.

8 | SUMMARY AND CONCLUSIONS

This paper investigated the collapse risk of seismically isolated buildings designed by the procedures of Section 17.3.3 of ASCE/SEI 7-16[9] for near-field ground motions based on a methodology proposed by Champion and Liel[27]. A building with an SCBF superstructure was designed with three different isolation systems that met the criteria for analysis and design of ASCE/SEI 7-16[9] for near-field ground motions. Two of the isolated buildings were designed with a large R_I factor (=1.8) and enhanced isolation system displacement capacity in the range of 1.3–1.6 times the maximum displacement D_{M} per ASCE/SEI 7-16[9]. The two isolation systems featured the same triple friction pendulum isolators[33] with the one having high friction sliding surfaces and the other having low friction sliding surfaces and enhanced with viscous dampers. The third isolation system features low friction triple friction pendulum bearings[33] of small displacement capacity equal to $1.1D_{\mathrm{M}}$ but with increased superstructure strength ($R_I = 1.1$). All isolation systems are acceptable per ASCE/SEI 7-16[9] but with the first two isolation systems expected to perform better due to their increased displacement capacity.

A probabilistic procedure was followed to generate collapse fragility curves that accounted for the probability of exceedance of pulse-like and non-pulse-like ground motions. Information on seismic hazard curves was obtained by PSHA and was used to compute collapse fragility curves for the three seismically isolated buildings. The probability of collapse given the $\mathrm{MCE_R}$ level earthquake was computed for the three isolation systems for various distances of the site to the fault, including far-field sites.

It was demonstrated that the collapse risk of seismically isolated buildings designed for near-field ground motions tends to slightly decrease with increasing site-to-source distance within the range of 0–4 km. It significantly decreased when the site is in the far-field. In general, the collapse probabilities given the $\mathrm{MCE_R}$ of the considered seismically isolated buildings, designed by the procedures of ASCE/SEI 7-16[9] for near-field ground motions, are less than 10% when the buildings are evaluated using near-field ground motions. The probabilities are several times smaller when the same buildings are evaluated using far-field ground motions. These probabilities of collapse are acceptable for buildings of risk category II per ASCE/SEI 7-16[9]. Note that further studies are needed that use more cases of seismically isolated building designs than investigated in this paper to observe what designs have acceptable collapse performance criteria per ASCE/SEI 7-16[9]. As the probabilities of collapse given the $\mathrm{MCE_R}$ for the three considered seismically isolated buildings are near 10% (especially for Isolation System 2), using smaller size isolators that have $D_{\mathrm{Capacity}} \approx D_{\mathrm{M}}$ or designing the superstructure with $R_{\mathrm{I}} \approx 2$ (especially for the Isolation System 3) will likely not result in acceptable collapse performance. Also, the current seismic design standard does not specify how many pulse-like records or non-pulse-like records (out of the total number of records to be used for design of seismically isolated buildings) to be used. The numbers of these records used for the design of the seismically isolated building may affect the design and thus its performance-thus it is worthy of study. Also, the record-to-record dispersion factor, β_{RTR}, for near field performance assessment warrants investigation.

The results show that the probabilities of collapse given the $\mathrm{MCE_R}$ have small differences for the three isolated buildings when evaluated using near-field ground motions, with the building with the high friction isolation system having the least collapse risk. Also, the building with the linear viscous damper enhanced isolation system had a noticeably lower probability of collapse given the $\mathrm{MCE_R}$ when evaluated using far-field ground motions. Evidently, the seismic isolation systems that have the best collapse performance for far-field motions are not necessarily the best for the near-field pulse-like ground motions.

ACKNOWLEDGEMENTS

The work of the first author was supported by funds of the Samuel P. Capen, Professorship at the University at Buffalo. The authors acknowledge the Baker Research Group at Stanford University for sharing on their website the pulse-like ground motion records[35] and MATLAB codes of the ground motion prediction model of Boore and Atkinson[52] and for classifying pulse and non-pulse like ground motions.

DATA AVAILABILITY STATEMENT

The data that support the findings of this study are available from the corresponding author upon reasonable request.

ORCID

Shoma Kitayama https://orcid.org/0000-0001-9416-3772

REFERENCES

1. Somerville PG, Smith NF, Graves RW, Abrahamson NA. Modification of empirical strong ground motion attenuation relations to include the amplitude and duration effects of rupture directivity. *Seismol Res Lett*. 1997;68(1):199–222.
2. Housner GW, Hudson DE. The Port Hueneme earthquake of March 18, 1957. *Bull Seismol Soc Am*. 1958;48(2):163–168.
3. Bertero VV, Mahin SA, Herrera RA. Aseismic design implications of near-fault San Fernando earthquake records. *Earthquake Eng Struct Dyn*. 1978;6:31–42.
4. Sekiguchi H, Irikura K, Iwata T. Determination of the location of faulting beneath Kobe during the 1995 Hyogo-ken Nanbu, Japan, earthquake from near-source particle motion. *Geophys Res Lett*. 1996;23(4):387–390.
5. Kamae K, Irikura K. Source model of the 1995 Hyogoken-Nanbu earthquake and simulation of near-source ground motion. *Bull Seismol Soc Am*. 1998;88(2):400–412.
6. Shahi SK, Baker JW. An efficient algorithm to identify strong-velocity pulses in multicomponent ground motions. *Bull Seismol Soc Am*. 2014;104(5):2456–2466.
7. Almufti I, Motamed R, Grant DN, Willford M. Incorporation of velocity pulses in design ground motions for response history analysis using a probabilistic framework. *Earthquake Spectra*. 2015;31(3):1647–1666.
8. Kohrangi M, Vamvatsikos D, Bazzurro P. Pulse-like versus non-pulse-like ground motion records: spectral shape comparisons and record selection strategies. *Earthquake Eng Struct Dyn*. 2019;48(1):46–64.
9. American Society of Civil Engineers (ASCE). *ASCE/SEI 7-16 Minimum Design Loads and Associated Criteria for Buildings and Other Structures*. American Society of Civil Engineers; 2017:822.
10. Liel AB, Luco N, Raghunandan M, Champion CP, Modifications to risk-targeted seismic design maps for subduction and near-fault hazards. 12th International Conference on Applications of Statistics and Probability in Civil Engineering, ICASP12 Vancouver, Canada, July 12–15; 2015.
11. Hall J, Ryan KL. Isolated building and the 1997 UBC near-source factors. *Earthquake Spectra*. 2000;16(2):393–411.
12. International Conference of Building Officials (ICBO). *Uniform Building Code Volume 2*. International Conference of Building Officials (International Code Council); 1997:574.
13. Kitayama S, Constantinou MC. *Seismic Performance Assessment of Seismically Isolated Buildings Designed by the Procedures of ASCE/SEI 7. Report MCEER-18-0004*. Multidisciplinary Center for Earthquake Engineering Research. University at Buffalo, The State University of New York; 2018:164.
14. Kitayama S, Constantinou MC. Collapse performance of seismically isolated buildings designed by the procedures of ASCE/SEI 7. *Eng Struct*. 2018; 164:243–258.
15. Shao B, Mahin SA, Zayas V. Achieving targeted levels of reliability for low-rise seismically isolated structures. *Soil Dyn Earthquake Eng*. 2019;125: 105744.
16. Masroor A, Mosqueda G. Assessing the collapse probability of base-isolated buildings considering pounding to moat walls using the FEMA P695 methodology. *Earthquake Spectra*. 2015;31(4):2069–2086.
17. American Society of Civil Engineers (ASCE). *ASCE/SEI 7-05 Minimum Design Loads for Buildings and Other Structures*. American Society of Civil Engineers; 2006:388.
18. Federal Emergency Management Agency (FEMA). Quantification of Building Seismic Performance Factors. Report FEMA P695. Federal Emergency Management Agency; 2009:422.
19. Bao Y, Becker TC, Sone T, Hamaguchi H. To limit forces or displacements: collapse study of steel frames isolated by sliding bearings with and without restraining rims. *Soil Dyn Earthquake Eng*. 2018;112:203–214.
20. Kitayama S, Constantinou MC. Further Results on the Assessment of Performance of Seismically Isolated Electrical Transformers. Report MCEER-20-0002. Multidisciplinary Center for Earthquake Engineering Research. University at Buffalo, The State University of New York; 2020:248.
21. Pant DR, Constantinou MC, Wijeyewickrema AC. Re-evaluation of equivalent lateral force procedure for prediction of displacement demand in seismically isolated structures. *Eng Struct*. 2013;52:455–465.
22. Vassiliou MF, Tsiavos A, Stojadinović B. Dynamics of inelastic base-isolated structures subjected to analytical pulse ground motions. *Earthquake Eng Struct Dyn*. 2013;42(14):2043–2060.
23. Bao Y, Becker TC, Hamaguchi H. Failure of double friction pendulum bearings under pulse-type motions. *Earthquake Eng Struct Dyn*. 2017;46(5):715–732.
24. Ricker N. Wavelet functions and their polynomials. *Geophysics*. 1944;9(3):314–323.
25. Akkar S, Yazgan U, Gulkan P. Drift estimates in frame buildings subjected to near-fault ground motions. *J Struct Eng*. 2005;131(7):1014–1024.

26. Ruiz-García J. Inelastic displacement ratios for seismic assessment of structures subjected to forward-directivity near-fault ground motions. *J Earthquake Eng*. 2011;15(3):449–468.
27. Champion C, Liel A. The effect of near-fault directivity on building seismic collapse risk. *Earthquake Eng Struct Dyn*. 2012;41(10):1391–1409.
28. Kitayama S, Constantinou MC. Effect of displacement restraint on the collapse performance of seismically isolated buildings. *Bull Earthquake Eng*. 2019;17:2767–2786.
29. Kitayama S, Constantinou MC. Probabilistic seismic performance assessment of seismically isolated buildings designed by the procedures of ASCE/SEI 7 and other enhanced criteria. *Eng Struct*. 2019;179:566–582.
30. Bao Y, Becker TC. Effect of design methodology on collapse of friction pendulum isolated moment-resisting and concentrically braced frames. *J Struct Eng ASCE*. 2018;144(11):04018203.
31. Structural Engineers Association of California (SEAOC). *2012 IBC SEAOC Structural/Seismic Design Manual Volume 5: Examples for Seismically Isolated Buildings and Buildings with Supplemental Damping*. Structural Engineers Association of California; 2014:170.
32. McVitty WJ, Constantinou MC. *Property Modification Factors for Seismic Isolators: Design Guidance for Buildings. Report MCEER-15-0005*. Multidisciplinary Center for Earthquake Engineering Research. University at Buffalo, The State University of New York; 2015:242.
33. Fenz DM, Constantinou MC. Spherical sliding isolation bearings with adaptive behavior: theory. *Earthquake Eng Struct Dyn*. 2008;37(2):163–183.
34. Computers and Structures Inc. *SAP2000®: Integrated finite element analysis and design of structures, version 21.2.0, software*. Computers and Structures Inc.; 2019.
35. Baker JW. Quantitative classification of near-fault ground motions using wavelet analysis. *Bull Seismol Soc Am*. 2007;97(5):1486–1501.
36. Kitayama S, Constantinou MC. Seismic performance of buildings with viscous damping systems designed by the procedures of ASCE/SEI 7-16. *J Struct Eng*. 2018;144(6):04018050.
37. Constantinou MC, Whittaker AS, Kalpakidis Y, Fenz DM, Warn GP. *Property Modification Factors for Seismic Isolators: Design Guidance for Buildings. Report MCEER-07-0012*. Multidisciplinary Center for Earthquake Engineering Research. University at Buffalo, The State University of New York; 2015:468.
38. McKenna FT, *Object-oriented Finite Element Programming: Frameworks for Analysis, Algorithms and Parallel Computing. Ph.D. Thesis*. University of California, Berkeley, CA, USA; 1997:247.
39. Shahi SK, Baker JW. An empirically calibrated framework for including the effects of near-fault directivity in probabilistic seismic hazard analysis. *Bull Seismol Soc Am*. 2011;101(2):742–755.
40. Ancheta TD, Darragh RB, Stewart JP, et al. *PEER NGA-West2 Database. PEER 2013/03*. Pacific Earthquake Engineering Research Center, University of California, Berkeley; 2013:172.
41. Tzimas A, Kamaris G, Karavasilis TL, Galassco C. Collapse risk and residual drift performance of steel buildings using post-tensioned MRFs and viscous dampers in near-fault regions. *Bull Earthquake Eng*. 2016;14(6):1643–1662.
42. Song B, Galasso C. Directivity-induced pulse-like ground motions and fracture risk of pre-Northridge welded column splices. *J Earthquake Eng*. 2020. https://doi.org/10.1080/13632469.2020.1772154.
43. Vamvatsikos D, Cornell CA. Incremental dynamic analysis. *Earthquake Eng Struct Dyn*. 2002;31(3):491–514.
44. Kitayama S, Constantinou MC. Probabilistic collapse resistance and residual drift assessment of buildings with fluidic self-centering systems. *Earthquake Eng Struct Dyn*. 2016;45(2):1935–1953.
45. Sabelli R, Roeder CW, Hajjar JF. *Seismic Design of Steel Special Concentrically Braced Frame Systems – A Guide for Practicing Engineers. NEHRP Seismic Design Technical Brief No. 8, NIST GCR 13-917-24*. National Institute of Standards and Technology; 2013:36.
46. Kitayama S, Lee D, Constantinou MC, Kempner L. Probabilistic seismic assessment of seismically isolated electrical transformers considering vertical isolation and vertical ground motion. *Eng Struct*. 2017;152:888–900.
47. Lee D, Constantinou MC. Combined horizontal-vertical seismic isolation system for high-voltage-power transformers: development, testing and validation. *Bull Earthquake Eng*. 2018;16:4273–4296.
48. Haselton CB, Baker JW, Liel AB, Deierlein GG. Accounting for ground-motion spectral shape characteristics in structural collapse assessment through an adjustment for epsilon. *J Struct Eng*. 2011;137(3):332–344.
49. Han SW, Wen YK. Method of Reliability-Based Calibration of Seismic Structural Parameters. Report SRS-595. UIUC-ENG-94. College of Engineering, University of Illinois at Urbana-Champaign; 1994:170.
50. Baker JW, Measuring bias in structural response caused by ground motion scaling. 8th Pacific Conference on Earthquake Engineering; 2007; Singapore; 056.
51. Baker JW, Cornell CA. Vector-valued intensity measures for pulse-like near-fault ground motions. *Eng Struct*. 2008;30(4):1048–1057.
52. Boore DM, Atkinson GM. Ground-motion prediction equations for the average horizontal component of PGA, PGV, and 5%-Damped PSA at spectral periods between 0.01 s and 10.0 s. *Earthquake Spectra*. 2008;24(1):99–138.
53. McGuire RK. Probabilistic seismic hazard analysis: early history. *Earthquake Eng Struct Dyn*. 2008;37(3):329–338.
54. Tothong P, Cornell CA, Baker JW. Explicit directivity-pulse inclusion in probabilistic seismic hazard analysis. *Earthquake Spectra*. 2007;23(4):867–891.
55. Chiou BR, Darragh N, Gregor N, Silva W. NGA project strong-motion database. *Earthquake Spectra*. 2008;24(1):23–44.
56. Kramer SL. *Geotechnical Earthquake Engineering*. Prentice Hall; 1996:653.
57. Baker JW. Introduction to Probabilistic Seismic Hazard Analysis. White Paper Version 2.0.1. Civil and Environmental Engineering, Stanford University; 2013:79. https://scits.stanford.edu/sites/g/files/sbiybj13751/f/baker_2013_intro_psha_v2.pdf

58. Eads L, Miranda E, Lignos DG. Average spectral acceleration as an intensity measure for collapse risk assessment. *Earthquake Eng Struct Dyn*. 2015;44(12):2057–2073.
59. Federal Emergency Management Agency (FEMA). Seismic Performance Assessment of Buildings Volume 1 – Methodology. Second edition. FEMA P-58-1. Federal Emergency Management Agency; 2018:340.
60. Kitayama S, Cilsalar H. Seismic loss assessment of seismically isolated buildings designed by the procedures of ASCE/SEI 7-16. *Bull Earthquake Eng*. 2021. https://doi.org/10.1007/s10518-021-01274-y.

How to cite this article: Kitayama S, Constantinou MC. Performance evaluation of seismically isolated buildings near active faults. *Earthquake Engng Struct Dyn*. 2022;51:1017–1037. https://doi.org/10.1002/eqe.3602